Progress In Electromagnetics Research, Vol. 134, 397–417, 2013

A NOVEL MINIATURIZED DUAL-BAND BANDSTOP FILTER USING DUAL-PLANE DEFECTED STRUCTURES

Jun Wang[1], Huansheng Ning[1, *], Qingxu Xiong[1], Minquan Li[2], and Lingfeng Mao[3]

[1]School of Electronic and Information Engineering, Beihang University, Beijing 100191, China

[2]School of Electronics and Information Engineering, Anhui University, Hefei, Anhui 230039, China

[3]Institute of Intelligent Structure and System, Soochow University, Suzhou, Jiangsu 215006, China

Abstract—A novel miniaturized dual-band bandstop filter (DBBSF) is proposed by using the T-shaped defected microstrip structures (DMSs) and the U-shaped defected ground structures (DGSs) in this paper. The layout of the dual-band bandstop resonator (DBBSR) is presented at first. The dual stopbands of the DBBSR can be separately controlled since the mutual coupling of the defected structures is negligible. The working principles of the T-shaped DMS and U-shaped DGS are then provided and their design process is summarized. On the basis of the DBBSR, the design methodology of the compact DBBSF is proposed before its design procedures are presented. Following the design procedures, a second-order and third-order DBBSFs with Butterworth frequency response are designed, simulated and fabricated. The equivalent circuit models of the designed filters are also developed. Full-wave simulation results of the fabricated DBBSFs are in good agreement with the circuit simulation and measurement results, validating our proposed design methodology.

1. INTRODUCTION

Bandstop filters have been widely used in many applications to block unwanted signals while allowing useful signals to pass through [1–4]. Recently, there is an increasing interest in the implementation of

Received 23 October 2012, Accepted 26 November 2012, Scheduled 5 December 2012

* Corresponding author: Huansheng Ning (ninghuansheng@buaa.edu.cn).

dual-band bandstop filters (DBBSFs) [5–12] since they can effectively suppress the undesired concurrent interference at two separate frequencies. It is demonstrated that [5] the DBBSF has a more compact size, lower cost, less passband insertion loss and lower group delay compared with a simple cascade of two conventional single-band bandstop filters.

Many different filter configurations based on planar technology have been proposed to implement DBBSF. In [5], the dual stopbands are synthesized by applying frequency-variable transformation to the lowpass prototype. Most recent research has been focused on size reduction of DBBSF, which may be achieved by using two-section [6] or three-section [7] stepped-impedance resonators (SIRs), or a dual-mode loop resonator [8]. The compact DBBSFs may also be realized by using a single end-shorted parallel coupled microstrip line and open-ended SIRs [9], or combining a spur-line structure and a rectangle slot [10]. However, it is not convenient to adjust the center frequency of each stopband for above filters. In order to solve that problem, the open-loop resonators with different length coupled to the main microstrip line are utilized at the expense of a relatively larger size [11]. The DBBSF composed of the meandered slot defected microstrip structure and the simplified spiral microstrip resonator is developed in [12] to obtain the independently controlled stopbands and improved spurious response. Nevertheless, the realization of a more compact DBBSF with high performance and conveniently adjusted stopbands is still an ongoing challenge.

Due to their prominent stopbands, spurious resonance suppression and slow-wave effects, the defected ground structure (DGS) and the defected microstrip structure (DMS) have been widely used for many microwave components design [13–19], especially for the miniaturized bandstop filter design [13, 14, 18]. By using above unique characteristics, a miniaturized DBBSF is developed by adopting the T-shaped DMS and U-shaped DGS in our previous work [20]. However, the design of the defected structures is not conducted and remains challenging. This is because that for a required frequency response, the dimensions of defected structure usually have to be speculated and then varied iteratively by an EM solver on a trial and error basis [21]. Moreover, a clear design procedure of this DBBSF should be also investigated.

The purpose of this paper is to present the efficient design of the T-shaped DMS and U-shaped DGS, as well as the design methodology of miniaturized DBBSF using dual-plane defected structures. Firstly, the configuration of the dual-band bandstop resonator (DBBSR) is presented. To provide a useful guide to the DBBSF design, the mutual

coupling of the defected structures of the DBBSR is analyzed in detail. Physical explanations of the defected structures are then given to obtain their operation principles. Secondly, a miniaturized DBBSF is developed based on above investigations, and its design methodology is carried out. To validate that, a second-order and third-order DBBSFs are designed following the presented design procedures, and the implemented filters are simulated and measured. Furthermore, the simulations of the individual T-shaped DMSs and U-shaped DGSs are performed and the equivalent circuit models of the designed DBBSFs are constructed to further investigate the mutual coupling of the defected structures. Finally, a comparison of previous DBBSFs and our proposed ones is drawn.

2. ANALYSIS OF THE DUAL-BAND BANDSTOP RESONATOR

2.1. Configuration

The layout of the presented DBBSR is shown in Fig. 1, where the T-shaped patterned structure is etched in the signal strip of the top plane and the U-shaped patterned structure is etched in the bottom ground plane. The adoption of this configuration is based on the obvious stopbands and slow-wave effects of our proposed T-shaped DMS in [20] and the U-shaped DGS in [13], as well as the negligible mutual coupling of these two structures which will be demonstrated in the following. For compactness, the first stopband is determined by the T-shaped DMS and the second stopband is dependent on the U-shaped DGS.

The Arlon Cuclad 250 (tm) substrate with a relative dielectric

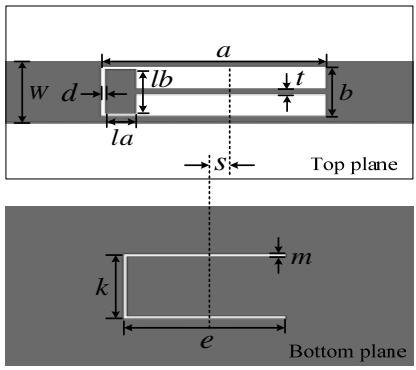

Figure 1. Configuration of the dual-band bandstop resonator.

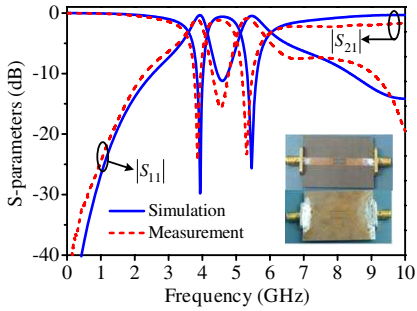

Figure 2. Simulated and measured S-parameters of the fabricated DBBSR. ($W = 4.5\,\text{mm}$, $a = 9.0\,\text{mm}$, $b = 3.6\,\text{mm}$, $d = 0.2\,\text{mm}$, $la = 1.2\,\text{mm}$, $lb = 3.2\,\text{mm}$, $t = 0.6\,\text{mm}$, $m = 0.3\,\text{mm}$, $k = 4.5\,\text{mm}$, $e = 9.0\,\text{mm}$, $s = 0\,\text{mm}$).

constant of 2.55 and a thickness of 1.5 mm is used in all the following simulations and fabrications. The width of the main microstrip line is chosen to be 4.5 mm corresponding to a characteristic impedance of 50 Ω. The simulated and measured results of the fabricated DBBSR are depicted in Fig. 2 and good agreement is obtained between the two. As can be seen from this figure, two prominent stopbands are centered at 3.94 GHz and 5.44 GHz respectively with both the rejection levels better than 23 dB. Small resonant frequency shift between the simulation and measurement may be attributed to the fabrication error. The surface current distribution of the DBBSR at resonant frequencies are shown in Fig. 3(a) and Fig. 3(c). It can be found that in Fig. 3(a), the current flows around the T-shaped DMS at the lower resonant frequency; while in Fig. 3(c), the current is distributed along the slot of U-shaped DGS at the higher resonant frequency. This indicates that the first and second stopbands are generated by the T-shaped DMS and U-shaped DGS correspondingly.

2.2. Mutual Coupling Analysis of the Defected Structures

To provide a guide to the DBBSF design, the mutual coupling of the defected structures of the DBBSR needs to be analyzed. Firstly, the individual T-shaped DMS and U-shaped DGS with the same dimensions of the fabricated DBBSR resonate at 3.94 GHz and 5.43 GHz with the surface current distribution shown in Fig. 3(b) and Fig. 3(d) correspondingly. The resonant frequencies of the individual structures are almost the same with that of the DBBSR. Meanwhile, little interference exists between the two defected structures despite

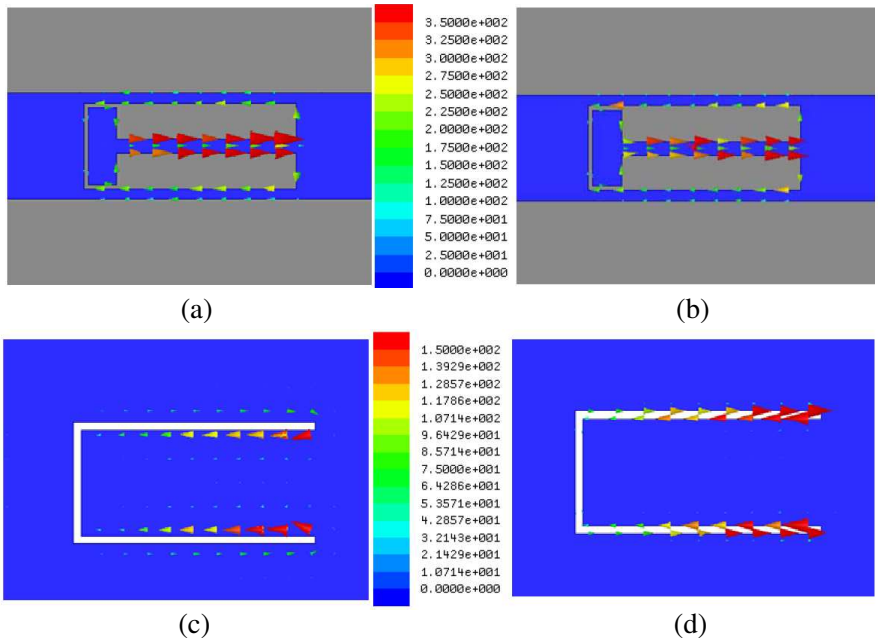

Figure 3. Simulated surface current distribution of different patterned structures. (a) The top plane of the DBBSR at 3.94 GHz. (b) The individual T-shaped DMS at 3.94 GHz. (c) The bottom plane of the DBBSR at 5.44 GHz. (d) The individual U-shaped DGS at 5.43 GHz.

a small current density difference when we compare Fig. 3(a) with Fig. 3(b), Fig. 3(c) with Fig. 3(d). Secondly, the effects of the T-shaped DMS length a and the U-shaped DGS length e on the resonant frequencies of the DBBSR are analyzed with the simulated results illustrated in Fig. 4. Fig. 4(a) shows that as a increases from 7 mm to 13 mm, the lower resonant frequency of DBBSR decreases from 4.66 GHz to 3.04 GHz while the higher resonance keeps invariant. In Fig. 4(b), it can be seen that when e varies from 6 mm to 12 mm, the higher resonant frequency of DBBSR decreases from 7.58 GHz to 4.22 GHz while the lower resonance remains unchanged. Moreover, the resonant frequencies of DBBSR are fully consistent with that of the individual structures in both Fig. 4(a) and Fig. 4(b). Finally, the influence of the relative longitudinal position s on the resonances of DBBSR is also analyzed. As depicted in Fig. 5, the lower and higher resonances keep almost the same as s varies, and the maximum deviations of the resonant frequency of the DBBSR from that of the individual T-shaped DMS and U-shaped DGS are only 0.07 GHz and

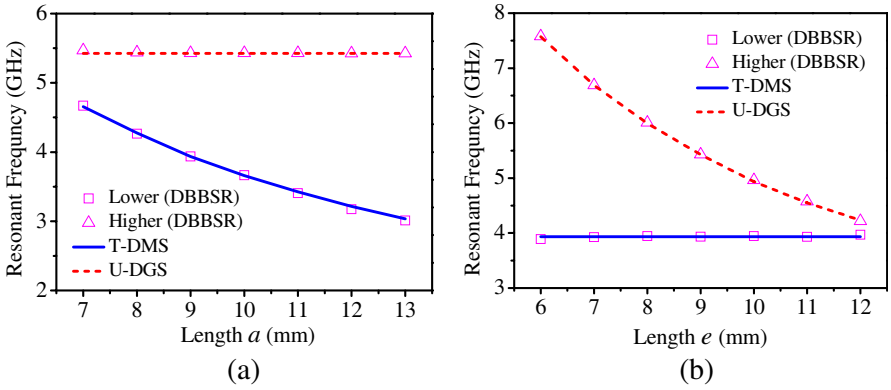

Figure 4. (a) Effects of the T-shaped DMS length a on the resonant frequencies of the DBBSR. (b) Effects of the U-shaped DGS length e on the resonant frequencies of the DBBSR.

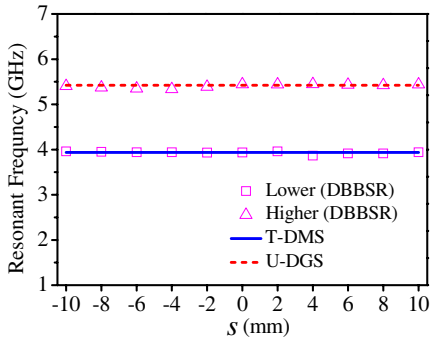

Figure 5. Variation of the lower and higher resonances of the DBBSR as a function of the relative longitudinal position s.

0.09 GHz. All analyses above demonstrate that the mutual coupling of the defected structures can be neglected, so that the dual stopbands can be individually controlled. The negligible mutual coupling may also be observed in the following full-wave and circuit simulations.

2.3. Operation Principles of the Defected Structures

2.3.1. T-shaped DMS

Figure 6(a) shows the equivalent circuit model of the T-shaped DMS. We assume that both the transmission lines at the bottom and top

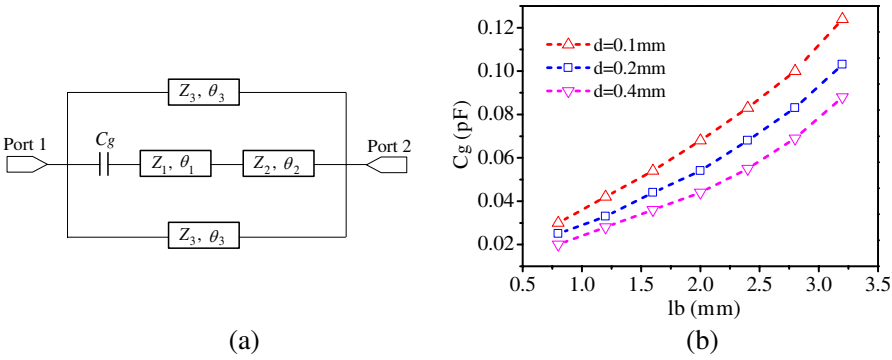

Figure 6. (a) Equivalent circuit model of the T-shaped DMS. (b) Coupling capacitance Cg as functions of the gap d and the width lb ($a = 9.0\,\text{mm}$, $b = 3.6\,\text{mm}$, $la = 1.2\,\text{mm}$, $t = 0.6\,\text{mm}$).

of the etched rectangle area have the characteristic impedance of Z_3 and the electrical length of θ_3. The left and right transmission lines in the etched rectangle area have the characteristic impedance of Z_1 and Z_2, and the electrical length of θ_1 and θ_2 respectively. The coupling capacitance Cg is introduced to describe the coupling between the T-shaped DMS and the main transmission line, which mainly depends on the gap d and the width lb. Using the network analysis theory, the reflection (S_{11}) and transmission coefficients (S_{21}) of the equivalent circuit model in Fig. 6(a) can be obtained as:

$$S_{11} = \frac{(Y_0 - Y_{11})(Y_0 + Y_{22}) + Y_{12}Y_{21}}{(Y_{11} + Y_0)(Y_{22} + Y_0) - Y_{12}Y_{21}} \tag{1}$$

$$S_{21} = \frac{-2Y_{21}Y_0}{(Y_{11} + Y_0)(Y_{22} + Y_0) - Y_{12}Y_{21}} \tag{2}$$

$$Y_{11} = D_1/B_1 - 2\mathrm{j}Y_3 \cot\theta_3 \tag{3}$$

$$Y_{12} = Y_{21} = -1/B_1 + 2\mathrm{j}Y_3 \csc\theta_3 \tag{4}$$

$$Y_{22} = A_1/B_1 - 2\mathrm{j}Y_3 \cot\theta_3 \tag{5}$$

where Y_0 is the port admittance, $Y_3 = 1/Z_3$, and the $ABCD$ parameters are

$$\begin{aligned} A_1 &= \cos\theta_1 \cos\theta_2 - Z_1Y_2 \sin\theta_1 \sin\theta_2 \\ &\quad + 1/\omega Cg\,(Y_1 \sin\theta_1 \cos\theta_2 + Y_2 \cos\theta_1 \sin\theta_2) \end{aligned} \tag{6}$$

$$\begin{aligned} B_1 &= \mathrm{j}\,(Z_2 \cos\theta_1 \sin\theta_2 + Z_1 \sin\theta_1 \cos\theta_2) \\ &\quad + \mathrm{j}/\omega Cg\,(Y_1Z_2 \sin\theta_1 \sin\theta_2 - \cos\theta_1 \cos\theta_2) \end{aligned} \tag{7}$$

$$C_1 = \mathrm{j}Y_1 \sin\theta_1 \cos\theta_2 + \mathrm{j}Y_2 \cos\theta_1 \sin\theta_2 \tag{8}$$

$$D_1 = -Y_1 Z_2 \sin\theta_1 \sin\theta_2 + \cos\theta_1 \cos\theta_2 \quad (9)$$

where $Y_1 = 1/Z_1$, and $Y_2 = 1/Z_2$.

Figure 6(b) depicts the variation of Cg when d or lb changes, which is obtained by comparing the circuit calculated results with the full-wave simulated results. As expected, Cg increases when d decreases or lb increases. It is worth pointing out that once this relation is constructed for a specific substrate, it can be used in the design of the T-shaped DMS directly. The full-wave simulated result and the circuit calculated result using (1) and (2) are shown in Fig. 7, where good agreement can be seen. A small discrepancy in the stopband bandwidth of the two is resulted from that the coupling between the transmission lines in the etched rectangle area (i.e., Z_1/θ_1 and Z_2/θ_2) and the transmission lines at the bottom and top of the etched rectangle area (i.e., Z_3/θ_3) is not included in Fig. 6(a). To give a better understanding of the operation principle of the T-shaped DMS, the effects of the dimensions on the transmission response are studied based on the following simulation results. We will place emphasis on the variation of 3-dB stopband bandwidth, which is a crucial parameter for the bandstop filter design [12, 22].

Figure 8(a) shows the transmission coefficients of the T-shaped DMS when the width b is varied while the rest of the dimensions remain constant. It is found that as b increases, a significant increase in the 3-dB fractional bandwidth (FBW) is obtained. This may be explained qualitatively as follows. The response of defected structure can be expressed by a parallel RLC circuit and the 3-dB FBW is proportional to $\sqrt{L/C}$ (L and C are the equivalent inductance and capacitance correspondingly) [13, 14]. From the surface current distribution shown

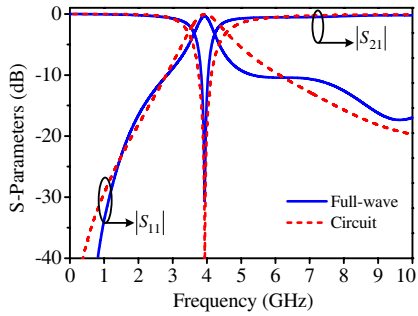

Figure 7. Comparison of S-parameters between the full-wave simulation and circuit calculation of the T-shaped DMS (The dimensions of the T-shaped DMS are the same with the fabricated DBBSR, Cg is 0.103 pF).

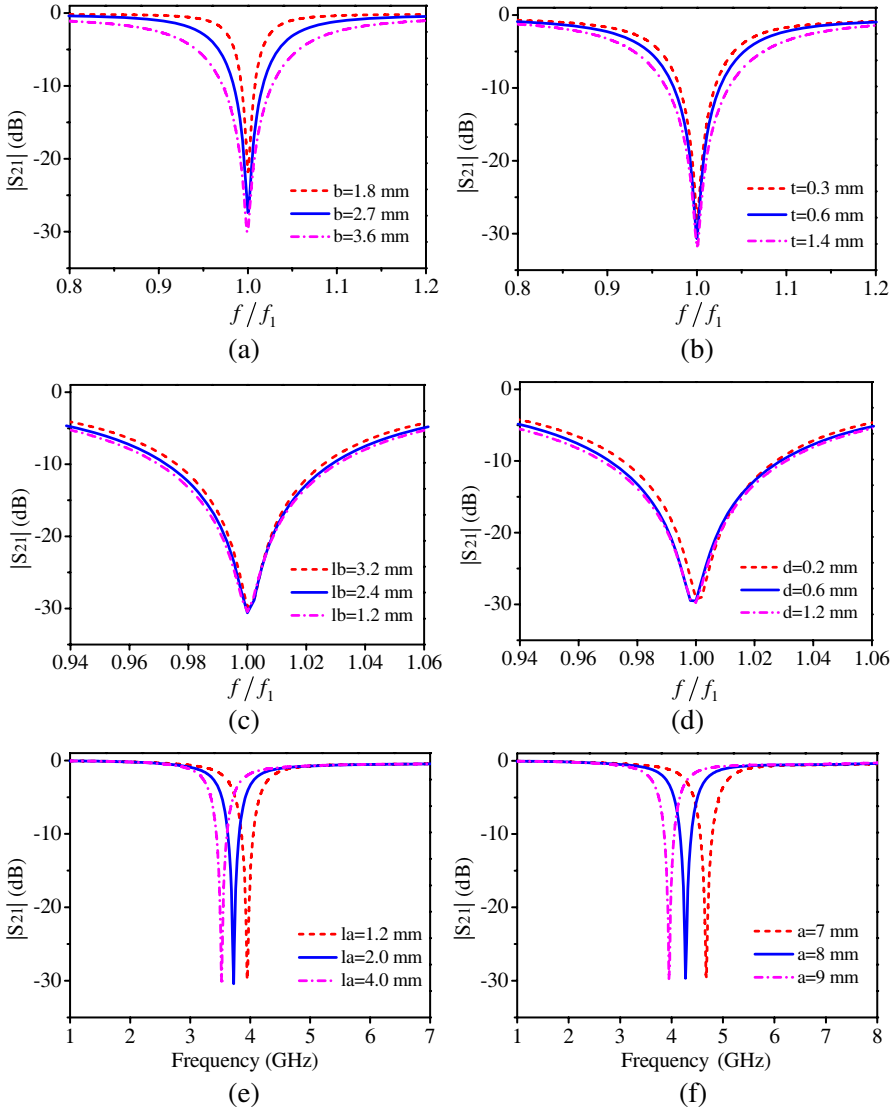

Figure 8. Variations of the transmission response for different T-shaped DMS (a) widths b ($lb = 1.6$ mm), (b) widths t, (c) widths lb, (d) gaps d, (e) lengths la and (f) lengths a (In the simulations, other dimensions of the T-shaped DMS are the same with the fabricated DBBSR unless specified otherwise, f_1 is the resonant frequency of the T-shaped DMS).

in Fig. 3(b), we can infer that for the T-shaped DMS, L is dependent on the length of the current path, whereas C is determined by the gaps of the transmission lines and the current density. The gaps and the current path increase with b, resulting in a decrease in C and an increase in L. Hence, the rapid change of the 3-dB FBW is understandable.

The S_{21}-parameters of the T-shaped DMS with a varied width t are plotted in Fig. 8(b), where the 3-dB FBW decreases with t. This is due to that as t decreases, the surface current density of the central line increases resulting in an increased C; however, the variation of C caused by the reduced gaps is neglected since b is large. Fig. 8(c) and Fig. 8(d) depict the simulated transmission responses of the T-shaped DMS when lb and d are separately changed. As can be seen in these two figures, both the variations of 3-dB FBW are slight because the influences of lb and d on C are small. The effect of the length la on the transmission coefficients is shown in Fig. 8(e). It is seen that when la increases from 1.2 mm to 4.0 mm, the resonant frequency of the T-shaped DMS decreases from 3.94 GHz to 3.51 GHz while the 3-dB bandwidth keeps almost unchanged (the variation of 3-dB bandwidth is only 0.08 GHz). This is resulted from the little change of C as la is varied. The same phenomenon may be also observed in Fig. 8(f) when a is changed.

The design of the T-shaped DMS can be conducted based on previous investigations. Initial dimensions can be obtained by the circuit calculation of Fig. 6(a). It is noticed that the dimension of b is chosen first since it mainly determines the stopband bandwidth. Then, the dimensions of t, lb and d may be slightly tuned by a full-wave EM solver to get the required 3-dB bandwidth. By properly adjusting la or a, the desired operation frequency can be achieved eventually.

2.3.2. U-shaped DGS

It has been demonstrated that the U-shaped DGS has a high Q factor and compact size in [13]. However, the physical understanding of this structure needs to be clarified to obtain its design rule. From the perspective of EM wave propagating, the U-shaped DGS can be regarded as a half guided wavelength crooked slot line resonator. Therefore, the resonant frequency f_2 may be achieved as:

$$f_2 = \frac{c}{2Lu\sqrt{\varepsilon_{slot}}} \tag{10}$$

where c is the free-space speed of light, $Lu = 2e + k$ the total length of the U-shaped DGS, ε_{slot} the effective dielectric constant of the slot and can be acquired by the closed-form equations in [23].

For the U-shaped DGS with the same dimensions of the fabricated DBBSR, the calculated resonant frequency using Eq. (10) is 5.42 GHz, nearly the same with the simulated resonant frequency of 5.43 GHz. The proposed analysis may be verified by the surface current distribution in Fig. 3(c) and Fig. 3(d) as well, where the current flows along the slot and two maximums occur at both ends of the slot, indicating that the total length of the U-shaped DGS corresponds to half guided wavelength at the resonant frequency.

The effects of the dimensions of the U-shaped DGS on the transmission response are investigated by the simulation results. Fig. 9(a) shows the simulated S_{21}-parameters when the width k of the U-shaped DGS is varied. We could find that a fast increase of the 3-dB FBW is obtained as k increases. The 3-dB FBW is slightly

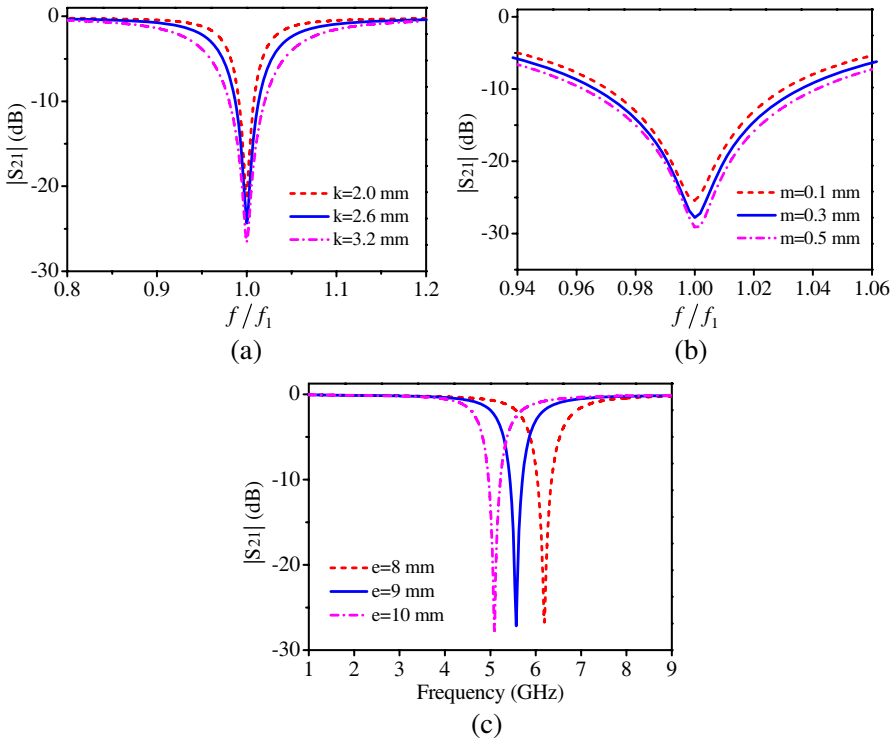

Figure 9. Effects of the U-shaped DGS (a) width k, (b) slot width m and (c) length e ($k = 3.6$ mm) on the transmission response (In the simulations, other dimensions of the U-shaped DGS are the same with the fabricated DBBSR unless specified otherwise).

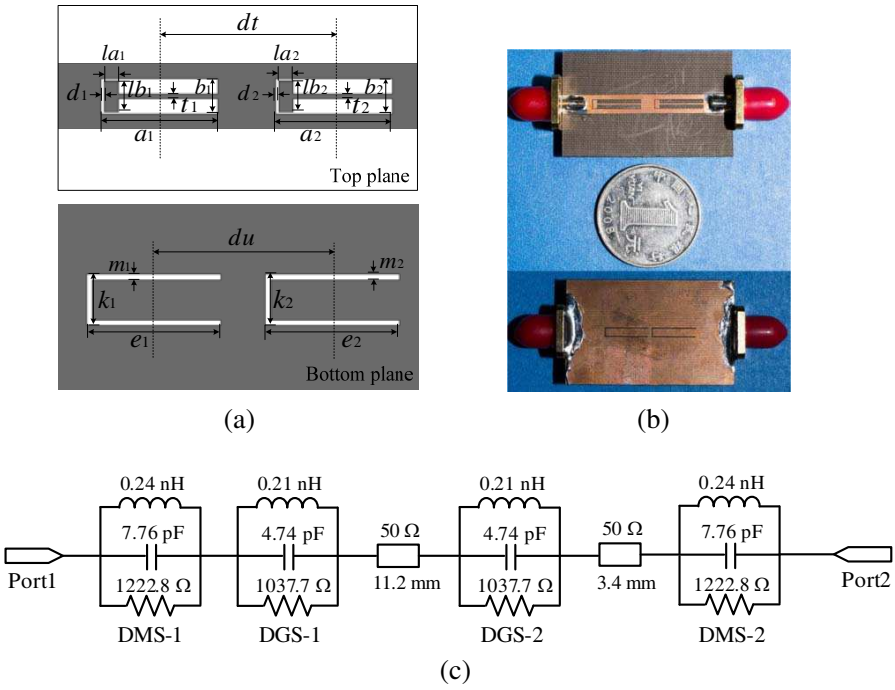

Figure 10. (a) Layout of the proposed second-order DBBSF. (b) Photograph of the fabricated filter. (c) Equivalent circuit model of the second-order filter. ($W = 4.5\,\text{mm}$, $a_1 = a_2 = 11.5\,\text{mm}$, $b_1 = b_2 = 2.3\,\text{mm}$, $d_1 = d_2 = 0.2\,\text{mm}$, $la_1 = la_2 = 1.0\,\text{mm}$, $lb_1 = lb_2 = 2.0\,\text{mm}$, $t_1 = t_2 = 0.3\,\text{mm}$, $dt = 14.6\,\text{mm}$, $m_1 = m_2 = 0.25\,\text{mm}$, $k_1 = k_2 = 2.3\,\text{mm}$, $e_1 = e_2 = 10.4\,\text{mm}$, $du = 11.2\,\text{mm}$.)

reduced when the slot width m decreases as shown in Fig. 9(b). The transmission coefficients of the U-shaped DGS with a varied e are plotted in Fig. 9(c). It can be observed that when e increases from 8 mm to 10 mm, the resonant frequency decreases from 6.19 GHz to 5.09 GHz whereas the variation of the 3-dB bandwidth is only 0.17 GHz. The explanations of above simulation results for the U-shaped DGS are not given here because it is similar to the T-shaped DMS. As for the design of the U-shaped DGS, the dimension of k is chosen first because it dominates the stopband bandwidth, while other dimensions can be estimated by using Eq. (10). Then, m and e may be slightly adjusted by a full-wave EM solver to obtain the desired 3-dB bandwidth at a given working frequency.

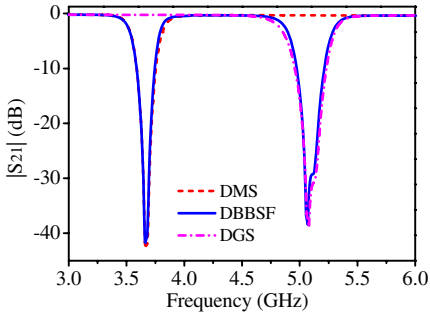

Figure 11. Full-wave simulated transmission responses of the second-order DBBSF as well as the individual T-shaped DMSs and U-shaped DGSs.

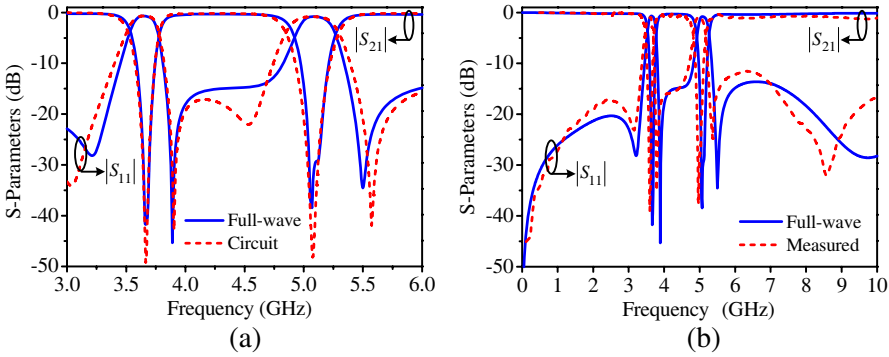

Figure 12. (a) Full-wave and circuit simulation results of the fabricated second-order filter. (b) Simulated and measured results of the second-order filter.

3. MINIATURIZED DBBSF DESIGN AND EXPERIMENTAL VERIFICATION

3.1. Filter Design Methodology

On the basis of the presented DBBSR, a miniaturized DBBSF can be further developed. Since the mutual coupling of the defected structures of the DBBSR is negligible as stated in the previous section, the design of DBBSF using dual-plane structures can be simplified to the design of each stopband using the T-shaped DMS or U-shaped DGS individually. Based on the conventional design method of bandstop filter [22], the design procedures of the proposed DBBSF are outlined as following:

Step 1: Determine the required normalized susceptance slope

parameters of each DMS and DGS through circuit synthesis. Using the given specifications of each stopband, i.e., the operated frequencies (f_1 and f_2) and the 3-dB FBWs (FBW_1 and FBW_2), the desired design parameters of the defected structures are calculated by

$$\frac{X_{1i}}{Y_0} = \frac{2\pi f_1 C_{1i}}{Y_0} = \frac{1}{2\pi f_1 L_{1i} Y_0} = \frac{f_1}{2\Delta f_{1-3\,\mathrm{dBi}}} = \frac{g_0}{g_i \Omega_c FBW_1},\ i = 1 \text{ to } n \quad (11)$$

$$\frac{X_{2i}}{Y_0} = \frac{2\pi f_2 C_{2i}}{Y_0} = \frac{1}{2\pi f_2 L_{2i} Y_0} = \frac{f_2}{2\Delta f_{2-3\,\mathrm{dBi}}} = \frac{g_0}{g_i \Omega_c FBW_2},\ i = 1 \text{ to } n \quad (12)$$

where X_{1i}/Y_0 and $\Delta f_{1-3\,\mathrm{dBi}}$ are the normalized susceptance slope parameters and 3-dB bandwidths of each T-shaped DMS correspondingly, X_{2i}/Y_0 and $\Delta f_{2-3\,\mathrm{dBi}}$ represents the normalized susceptance slope parameters and 3-dB bandwidths of each U-shaped DGS respectively, C_{1i} and C_{2i} are the equivalent capacitances of the defected structures, L_{1i} and L_{2i} are the equivalent inductances of the defected structures, g_i are the element values of lowpass prototype, Ω_c is the normalized cutoff frequency. For design simplicity, the characteristic admittances of the immitance inverters between the T-shaped DMSs or U-shaped DGSs are chosen to be the same with Y_0, and the dual stopbands have the same type of frequency response.

Step 2: Design the first stopband using the T-shaped DMSs. According to the required $\Delta f_{1-3\,\mathrm{dBi}}$ and the first operation frequency, the dimensions of each T-shaped DMS can be obtained following the design process in Section 2.3.1. The central distance between adjacent T-shaped DMSs is about a quarter of the guided wavelength at f_1. A fine-tuning process is often adopted to achieve an optimized performance.

Step 3: Design the second stopband using the U-shaped DGSs. Based on the desired $\Delta f_{2-3\,\mathrm{dBi}}$ and the second operation frequency, the dimensions of each U-shaped DGS may be achieved using the design steps in Section 2.3.2. The separation between adjacent U-shaped DGSs is about a quarter of the guided wavelength at f_2. The final optimized dimensions can be obtained with the aid of a full-wave EM solver.

To demonstrate the design methodology of the proposed DBBSF, a second-order and third-order DBBSF are implemented with the details given in following Section 3.2 and Section 3.3.

3.2. Second-order DBBSF Implementation

A DBBSF with the second-order Butterworth frequency response is designed with the following specifications. The center frequencies of the dual stopbands are $f_1 = 3.66\,\mathrm{GHz}$ and $f_2 = 5.07\,\mathrm{GHz}$, with

$FBW_1 = 7.91\%$ and $FBW_2 = 9.17\%$ respectively. The element values of the lowpass prototype are found to be $g_0 = g_3 = 1.0$, $g_1 = g_2 = 1.4142$. The desired normalized susceptance slope parameters are then obtained as:

$$X_{11}/Y_0 = X_{12}/Y_0 = 8.94, \quad X_{21}/Y_0 = X_{22}/Y_0 = 7.71 \tag{13}$$

The first T-shaped DMS (U-shaped DGS) has the same dimensions with the second one due to the equal required normalized susceptance slope parameter. Fig. 10(a) shows the configuration of the designed second-order filter. The final dimensions of this filter can be obtained following the design procedures of the DBBSF.

The simulated transmission responses of the second-order DBBSF and the individual defected structures are plotted in Fig. 11. It can be clearly seen that the first and second stopbands of the second-order DBBSF are in excellent agreement with the stopbands generated by the individual T-shaped DMSs and U-shaped DGSs respectively. This further indicates the negligible mutual coupling of the defected structures. The designed filter is fabricated and its photograph is presented in Fig. 10(b). The equivalent circuit model of the fabricated filter is also developed and illustrated in Fig. 10(c). It should be pointed out that the values of the circuit parameters are extracted from the T-shaped DMSs and U-shaped DGSs individually. The full-wave and circuit simulation results of the fabricated filter are shown in Fig. 12(a) and very good agreement between the two can be found. The fabricated filter is tested with an Agilent 8722ET network analyzer. The measured and simulated results are plotted in Fig. 12(b), where the simulation agrees well with the measurement. A slight shift in the resonant frequency may be resulted from the fabrication tolerance. As shown in Fig. 12(b), the first stopband is centered at 3.59 GHz with 3-dB FBW of 7.80% (3.45 GHz–3.73 GHz), and the second stopband is located at 4.97 GHz with 3-dB FBW of 8.85% (4.77 GHz–5.21 GHz). The measured rejection levels of the dual stopbands are 38.9 dB and 37.6 dB respectively. Detailed measured data show that the minimum insertion losses of the lower/middle/upper passbands are 0.05/0.30/0.72 dB correspondingly with the return loss better than 11.5 dB in the whole passbands.

3.3. Third-order DBBSF Implementation

To improve the stopband rejection of DBBSF, a third-order filter is also designed and implemented. The design specifications are $f_1 = 3.56$ GHz and $f_2 = 5.03$ GHz, with $FBW_1 = 7.96\%$ and $FBW_2 = 8.82\%$ respectively. The element values of the lowpass prototype with a third-order Butterworth frequency response are found

to be $g_0 = g_1 = g_3 = g_4 = 1.0$, $g_2 = 2.0$. Thus, the required normalized susceptance slope parameters are

$$X_{11}/Y_0 = X_{13}/Y_0 = 12.55,\ X_{12}/Y_0 = 6.28,$$
$$X_{21}/Y_0 = X_{23}/Y_0 = 11.34,\ X_{22}/Y_0 = 5.67 \tag{14}$$

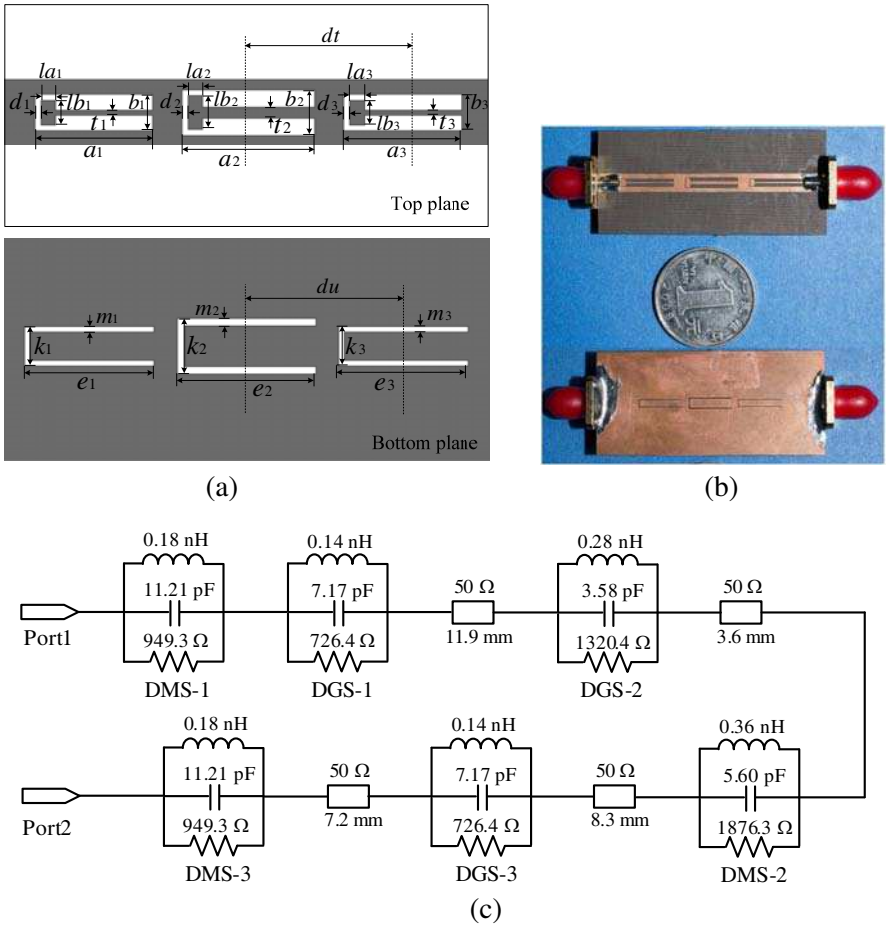

Figure 13. (a) Layout of the proposed third-order DBBSF. (b) Photograph of the fabricated filter. (c) Equivalent circuit model of the third-order filter. ($W = 4.5\,\text{mm}$, $a_1 = a_3 = 12.8\,\text{mm}$, $a_2 = 12.7\,\text{mm}$, $b_2 = 2.5\,\text{mm}$, $b_1 = b_3 = 1.9\,\text{mm}$, $d_1 = d_2 = d_3 = 0.2\,\text{mm}$, $dt = 15.5\,\text{mm}$, $la_1 = la_2 = la_3 = 1.0\,\text{mm}$, $lb_1 = lb_3 = 1.6\,\text{mm}$, $lb_2 = 2.2\,\text{mm}$, $t_1 = t_3 = 0.3\,\text{mm}$, $t_2 = 0.7\,\text{mm}$, $m_2 = 0.3\,\text{mm}$, $e_2 = 10.4\,\text{mm}$, $k_2 = 2.75\,\text{mm}$, $m_1 = m_3 = 0.25\,\text{mm}$, $k_1 = k_3 = 1.9\,\text{mm}$, $e_1 = e_3 = 10.6\,\text{mm}$, $du = 11.9\,\text{mm}$).

In this case, the dimensions of the first T-shaped DMS (U-shaped DGS) are equal to the third one, but different with the second one. Fig. 13(a) depicts the layout of the designed third-order filter with the dimensions obtained by previous design steps.

The simulated S_{21}-parameters of the third-order DBBSF and the individual defected structures are drawn in Fig. 14, where the stopbands caused by the individual T-shaped DMSs and U-shaped DGSs agree well with the first and second stopbands of the DBBSF correspondingly. The neglected mutual coupling of the defected structures is demonstrated again and our proposed design concept is further verified. Fig. 13(b) shows the photograph of the fabricated filter

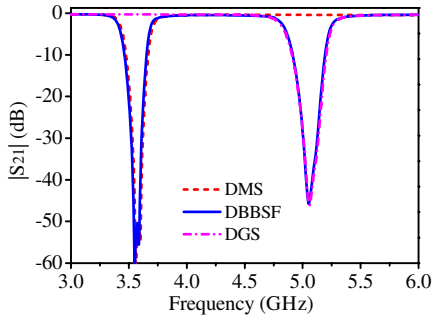

Figure 14. Full-wave simulated transmission responses of the third-order DBBSF as well as the individual T-shaped DMSs and U-shaped DGSs.

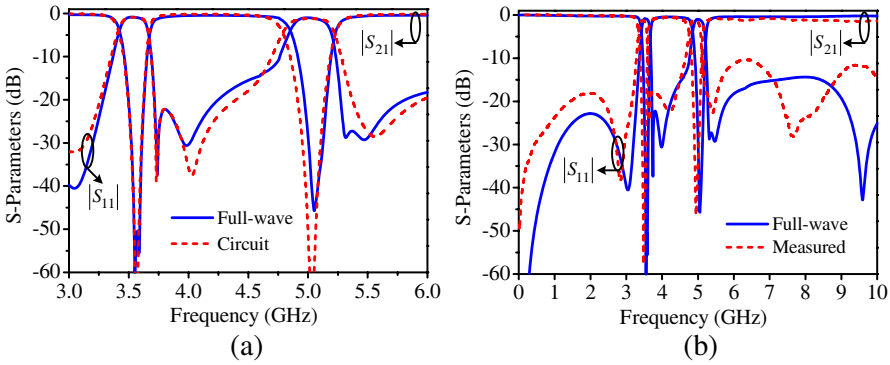

Figure 15. (a) Full-wave and circuit simulation results of the fabricated third-order filter. (b) Simulated and measured results of the third-order filter.

and the equivalent circuit model of this filter is given in Fig. 13(c). The values of the circuit parameters are still extracted from the T-shaped DMSs and U-shaped DGSs separately. Good agreement between the full-wave and circuit simulation is observed as shown in Fig. 15(a). Fig. 15(b) shows the measured and simulated results of the fabricated third-order filter, and the measurement is in reasonable agreement with the simulation. The measured dual stopbands are centered at 3.49 GHz and 4.95 GHz with 3-dB FBWs of 8.60% (3.33 GHz–3.63 GHz) and 8.69% (4.73 GHz–5.16 GHz), stopband rejections of 57.7 dB and 46.4 dB respectively. The minimum insertion losses of the lower/middle/upper passbands are 0.05/0.49/0.81 dB correspondingly with the return loss below −10.3 dB in the whole passbands.

3.4. Discussion

The comparison between the performances of previous DBBSFs and our proposed ones is made in Table 1. We may find that the proposed filters have two major advantages. First, one stopband is independent of another, which is one of the most important parameters in the implementation of dual-band applications. Second, the T-shaped DMSs and the U-shaped DGSs only occupy the space of the signal

Table 1. Comparison between the performances of previous DBBSFs and our proposed ones.

Ref.	Stopband 1 Freq. (GHz) /Rej. (dB)	Stopband 2 Freq. (GHz) /Rej. (dB)	Freely Controlled Stopbands	Passband Performance	Occupied Area (λg^2)
[6]	1.57/46.0	3.16/53.0	No	Normal	0.178
[7]	1.50/39.8	3.11/42.0	No	Normal	0.213
[8]	2.10/37.0	6.40/30.0	No	Normal	0.344
[9]	0.92/35.0	2.16/35.0	No	Good	0.096
[10]	2.12/**19.4**	2.90/**22.1**	No	Normal	0.034
[11]	1.55/22.5	2.65/40.0	Yes	Normal	0.427
[12]	2.37/31.4	3.54/36.7	Yes	Good	0.092
Prop. 1	3.59/38.9	4.97/37.6	Yes	Good	0.061
Prop. 2	3.49/57.7	4.95/46.4	Yes	Good	0.099

Freq. and Rej. represent the center frequency and rejection level of the stopband correspondingly. Passband performance denotes the insertion losses and return losses of the lower/middle/upper passbands. λg is the guided wavelength at the middle frequency between the first and the second stopband. Prop. 1 and Prop. 2 denote the proposed second-order and third-order DBBSF respectively.

strip and the ground plane, needing no extra space like other published filters. As the patterned structures are located along the direction of the transmission line, the proposed filters are even more compact. The occupied area of the proposed second-order filter is 66.7% of the most recently presented DBBSF in [12] but the stopband rejections are similar.

4. CONCLUSION

This paper proposes a novel miniaturized DBBSF using dual-plane defected structures. It is shown that the mutual coupling between the T-shaped DMS and the U-shaped DGS is negligible, making the dual stopbands convenient to adjust. The operation principles of the T-shaped DMS and U-shaped DGS are provided for efficient structure design. Based on these investigations, the design methodology of miniaturized DBBSF is proposed. By applying the presented design procedures, a second-order and third-order DBBSFs with Butterworth frequency response are demonstrated with both the simulated and measured results. The full-wave simulation, circuit simulation and measurement results of the fabricated filters agree well with each other. With individually adjusted stopbands, high performance and simple design procedures, the proposed miniaturized DBBSFs have great potential for practical applications.

ACKNOWLEDGMENT

This work is jointly funded by the National Natural Science Foundation of China (NSFC) and Civil Aviation Administration of China (CAAC) (61079019).

REFERENCES

1. Moghadasi, S. M., A. R. Attari, and M. M. Mirsalehi, "Compact and wideband 1-D mushroom-like EBG filters," *Progress In Electromagnetics Research*, Vol. 83, 323–333, 2008.
2. Wu, Y. and Y. Liu, "A coupled-line band-stop filter with three-section transmission-line stubs and wide upper pass-band performance," *Progress In Electromagnetics Research*, Vol. 119, 407–421, 2011.
3. Cui, D., Y. Liu, Y. Wu, S. Li, and C. Yu, "A compact bandstop filter based on two meandered parallel-coupled lines," *Progress In Electromagnetics Research*, Vol. 121, 271–279, 2011.

4. Xiang, Q.-Y., Q.-Y. Feng, and X.-G. Huang, "A novel microstrip bandstop filter and its application to reconfigurable filter," *Journal of Electromagnetic Waves and Applications*, Vol. 26, Nos. 8–9, 1039–1047, 2012.
5. Uchida, H., H. Kamino, K. Totani, N. Yoneda, M. Miyazaki, Y. Konishi, S. Makino, J. Hirokawa, and M. Ando, "Dual-band-rejection filter for distortion reduction in RF transmitters," *IEEE Trans. Microwave Theory Tech.*, Vol. 52, No. 11, 2550–2556, 2004.
6. Chin, K.-S., J. H. Yeh, and S. H. Chao, "Compact dual-band bandstop filters using stepped-impedance resonators," *IEEE Microwave Wireless Comp. Lett.*, Vol. 17, No. 12, 849–851, 2007.
7. Chin, K.-S. and C.-K. Lung, "Miniaturized microstrip dual-band bandstop filters using tri-section stepped-impedance resonators," *Progress In Electromagnetics Research C*, Vol. 10, 37–48, 2009.
8. Chiou, H.-K. and C.-F. Tai, "Dual-band microstrip bandstop filter using dual-mode loop resonator," *Electron. Lett.*, Vol. 45, No. 10, 507–509, 2009.
9. Velidi, V. K. and S. Sanyal, "Compact planar dual-wideband bandstop filters with cross coupling and open-ended stepped impedance resonators," *ETRI Journal*, Vol. 32, No. 1, 148–150, 2010.
10. Cheng, D., H.-C. Yin, and H.-X. Zheng, "A compact dual-band bandstop filter with defected microstrip slot," *Journal of Electromagnetic Waves and Applications*, Vol. 26, No. 10, 1374–1380, 2012.
11. Vegesna, S. and M. Saed, "Microstrip dual-band bandpass and bandstop filters," *Microw. Opt. Technol. Lett.*, Vol. 54, No. 1, 168–171, 2012.
12. Ning, H., J. Wang, Q. Xiong, and L. Mao, "Design of planar dual and triple narrow-band bandstop filters with independently controlled stopbands and improved spurious response," *Progress In Electromagnetics Research*, Vol. 131, 259–274, 2012.
13. Woo, D., T. Lee, J. Lee, C. Pyo, and W. Choi, "Novel U-slot and V-slot DGSs for bandstop filter with improved Q factor," *IEEE Trans. Microwave Theory Tech.*, Vol. 54, No. 6, 2840–2847, 2006.
14. Huang, S. Y. and Y. H. Lee, "A compact E-shaped patterned ground structure and its applications to tunable bandstop resonator," *IEEE Trans. Microwave Theory Tech.*, Vol. 57, No. 3, 657–666, 2009.
15. Liu, J. X., W. Y. Yin, and S. L. He, "A new defected ground structure and its application for miniaturized switchable antenna,"

Progress In Electromagnetics Research, Vol. 107, 115–128, 2010.

16. Barbarino, S. and F. Consoli, "UWB circular slot antenna provided with an inverted-L notch filter for the 5 GHz WLAN band," *Progress In Electromagnetics Research*, Vol. 104, 1–13, 2010.
17. Wang, C. J. and T. H. Lin, "A multi-band meandered slotted-ground-plane resonator and its application of low-pass filter," *Progress In Electromagnetics Research*, Vol. 120, 249–262, 2011.
18. Xiang, Q.-Y., Q.-Y. Feng, and X.-G. Huang, "Bandstop filter based on complementary split ring resonators defected microstrip structure," *Journal of Electromagnetic Waves and Applications*, Vol. 25, No. 13, 1895–1908, 2011.
19. Gao, M.-J., L.-S. Wu, and J. F. Mao, "Compact notched ultra-wideband bandpass filter with improved out-of-band performance using quasi electromagnetic bandgap structure," *Progress In Electromagnetics Research*, Vol. 125, 137–150, 2012.
20. Wang, J., H. Ning, L. Mao, and M. Li, "Miniaturized dual-band bandstop filter using defected microstrip structure and defected ground structure," *IEEE-MTT-S International Microw. Symp. Dig.*, 1–3, 2012.
21. Guha, D. and Y. M. M. Antar, *Microstrip and Printed Antennas: New Trends, Techniques and Applications*, John Wiley & Sons, New York, 2011.
22. Hong, J. S. and M. J. Lancaster, *Microstrip Filters for RF/Microwave Applications*, John Wiley & Sons, New York, 2001.
23. Gupta, K. C., R. Garg, I. Bahl, and P. Bhartia, *Microstrip Lines and Slotlines,* 2nd Edition, Artech House, Norwood, MA, 1996.